Gravity-assisted segregation of granular materials of equal mass and size

Johnrob Bantang, May Lim, Christopher Monterola, and Caesar Saloma*
National Institute of Physics, University of the Philippines, Diliman 1101, Quezon City, Philippines
(Received 23 July 2002; published 15 October 2002)

High-resolution segregation is demonstrated for elastic granular materials of the same mass and size. Each grain starts at a randomly selected position in the entrance facet of a cylinder, accelerates downwards due to gravity, and then bounces against a massive obstacle with a collision cross section that is proportional to the facet size. Bounce dynamics of the falling grain is a function of its relative elasticity with the obstacle. Subsequent collisions of the grain with the wall are assumed to be perfectly elastic. In the absence of interparticle collisions, grain focusing occurs at points along the cylinder axis. In the absence of rotation, focusing occurs regardless of the initial locations and (downward) velocities of the grains at the entrance facet. The focus location depends only on the coefficient of restitution of the falling particle and the obstacle size. Grains arrive at the focus in temporally localized bursts even if released simultaneously from the facet. Efficient segregation is, therefore, achieved without additional mechanical work (e.g., shaking, spinning) on the system configuration.

DOI: 10.1103/PhysRevE.66.041306 PACS number(s): 81.05.Rm, 83.10.Pp

I. INTRODUCTION

Granular matter is encountered in many aspects of daily life from food ingredients (e.g., sugar, cream, coffee, rice grains, cereals, etc.), medical tablets and capsules, facial powders, to construction materials (sand, gravel, cement). The possible sizes of granular materials encompass a wide range of scale from the submillimetric silica sand grains to meter-size rocks and boulders.

Granular matter is interesting because it could be considered as a new type of condensed matter that exhibit properties which are liquidlike, gaslike, and solidlike [1]. Granular materials could assume the shape of their container, support a load (in the absence of confinement) and its component particles do not exhibit noncontact interaction.

Rapid and accurate segregation and mixing are two important concerns when handling granular materials [2–12]. The capability to separate or mix different granular materials according to a desired specification has important applications in the service, utility, and manufacturing sectors of industry. Researchers have also found that a number of interesting phenomena could arise depending on the mixing or separation technique that is being utilized [2,3,8,11].

Granular materials are usually separated according to size or mass. Spatial (mesh) filter is the most straightforward method for rapid size separation. Grains of different mass or size values may also be separated by spinning, shaking, rolling, or sliding [8,10,11,13–15]. Granular materials could also be distinguished by their elastic property which becomes useful when dealing with grains of the same mass and size. Differences in elasticity between grains were found to be sufficient to result in the formation of patterns via shaking along different directions [12].

In this paper, we demonstrate a simple configuration that permits the separation at high resolution, of grains of the same mass and size but different elastic properties. Efficient segregation is achieved without additional mechanical work (e.g., shaking, spinning) on the system configuration which consists of cylindrical pipe of radius R_c with its axis directed towards ground (see, Fig. 1). Located a distance H from the entrance facet of radius R_e, is a massive (spheroid) obstacle of mass M_o and radius R_o, whose center is located on the cylinder axis. A grain of mass M_g ($\ll M_o$) and radius R_g, enters the pipe at a random position in the entrance facet, accelerates downward due to gravity and collides with the

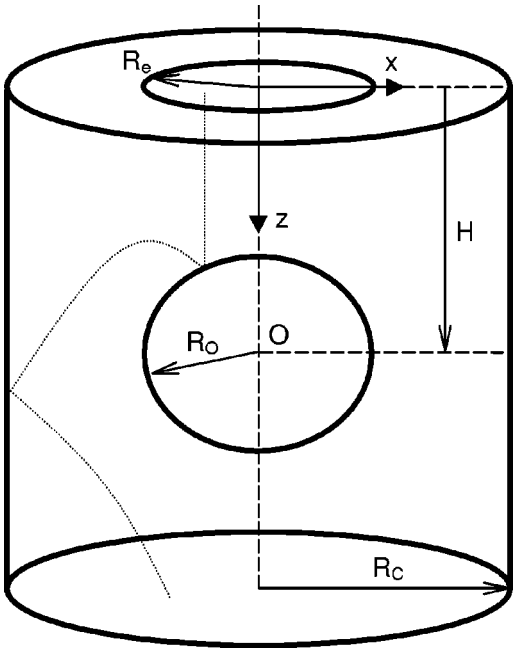

FIG. 1. Simple system for segregating particles of the same mass and size but different elasticity. Particles are released at randomly chosen locations in the entrance facet at $z=0$, accelerate downwards due to gravity, and strike an obstructing spheroid of mass $M_o \gg M_g$. Center O of the spheroid is located at $z=H$ and its spheroid radius $R_o < R_c$. Since $R_e = R_o$, every falling particle strikes the obstacle at least once. The dotted curve represents a typical trajectory of the particle.

*Electronic address: csaloma@nip.upd.edu.ph

spheroid. The bounce behavior of the grain is influenced by its elasticity relative to the spheroid obstacle and can result to subsequent (elastic) collisions with the cylindrical wall and the obstacle at later times.

In the absence of interparticle collision ($R_g \to 0$), the configuration leads to a natural focusing of the falling grains at points along the cylinder axis. The specific focus location depends only on the coefficient of restitution of the falling grain and the massive obstacle. It is independent of the initial locations at the entrance facet. An efficient segregation process is, therefore, realized without additional mechanical work (e.g., shaking, spinning) given to the system. To our knowledge such kind of systems has attracted minimal attention since the Galton board which is a two-dimensional arrangement of pegs that resembles a crystalline structure [16].

The focusing behavior of the falling grains are investigated in both space and time. We compare the results that are obtained via a massive spheroid with that of an equally-massive conic obstacle. The configuration at hand represents a filter design that is economical, efficient, and easy to maintain. The segregation dynamics that is determined could also provide new insights into the behavior of complicated real systems such as cascading rocks and debris.

The rest of the paper is organized as follows: In Sec. II we present a derivation of the governing equations of motion of the falling grain and the results of the numerical experiments are presented and analyzed in Secs. III and IV, respectively.

II. FORMULATION

A. General

The trajectory $\vec{r}=\vec{r}(x,y,z,t)$ of a point particle that is under the influence of force $\vec{F}$ and which undergoes a K number of collisions during flight, is described by

$$M_g d^2\vec{r}/dt^2 = \sum_k \vec{J}_k \delta(t-t_k) + \vec{F}(\vec{r}, d\vec{r}/dt, t), \tag{1}$$

where M_g is the particle mass, t is time, $\vec{J}_k$ represents the impulse that is generated during the kth collision, $\delta()$ is the Dirac delta function, t_k is the time of collision, and index $k=1,2,\ldots,K$. The particle is initially ($t=0$) at location $z=z_o$.

In terms of the tangential (T) and normal (N) components of the incident momentum $\vec{p}_k = M_g \vec{v}_k$, of the particle at the moment of the kth collision, the impulse $\vec{J}_k$ is given by

$$\vec{J}_k = (\mu_T - 1)\vec{p}_k^{(T)} - (\mu_N + 1)\vec{p}_k^{(N)}, \tag{2}$$

where $\vec{p}_k = \vec{p}_k^{(T)} + \vec{p}_k^{(N)}$ [10]. The presence of a nonzero normal coefficient of restitution μ_N causes the linear momentum of the particle to change and to lose energy ($0 \leqslant \mu_N \leqslant 1$). On the other hand, the presence of a tangential component μ_T can lead to a possible spinning of the particle ($-1 < \mu_T < 1$). Nonzero μ_N and μ_T values imply the presence of elasticity and friction between the two interacting surfaces. A collision is elastic when $\mu = 1.0$ and perfectly inelastic when $\mu = 0$.

A moving particle collides with a fixed (massive) three-dimensional obstacle O and the (outer) wall W which are described by surfaces $Q_o(\vec{r})=0$ and $Q_w(\vec{r})=0$, respectively. The instances of collisions $\{t_k\}$ are time solutions to $Q_o(\vec{r}(t_k))=0$, or $Q_w(\vec{r}(t_k))=0$.

In this work we assume that: (i) $\vec{F}=m\vec{g}$, where $\vec{g}$ is gravitational acceleration and (ii) System configuration consists of a cylindrical pipe and a massive obstacle of radius R_o that is oriented along the cylinder axis (see, Sec. I). The three-dimensional wall profile of the pipe is described by $Q_w(\rho,z,\theta)=\rho-\rho_w=0$, where: $\rho_w > R_o$. Two kinds of solid obstacles are considered—the spheroid and the cone which are described respectively by

$$Q_o(\rho,z,\theta) = \rho^2 + z^2 - R_o^2 = 0 \tag{3a}$$

and

$$Q_o(\rho,z,\theta) = \rho \tan\theta + z = 0. \tag{3b}$$

For the cone, we have $\rho < R_o$ and θ as the angle of the cone with respect to the horizontal. Figure 1 shows the geometrical configuration for the case of a spheroid obstacle.

B. Numerical implementation

The trajectory of the mth falling particle ($R_g=0$) is tracked using Eq. (1) in the case of a uniform force field $\vec{F}=m\vec{g}$, until it crosses a certain transverse plane $z=z_h$ down the pipe where index $m=1,2,\ldots,M$. The most recent position of a particle is given by

$$\vec{r}_{m,q+1} = \vec{r}_{m,q} + \vec{v}_{m,q}\delta t + 0.5\vec{g}\,\delta t^2, \tag{4}$$

where $\vec{r}_{m,q}$ and $\vec{v}_{m,q}$ are the position and velocity of the mth particle after the qth iteration, and δt is the time duration that it takes for the particle to change position from $\vec{r}_{m,q}$ to $\vec{r}_{m,q+1}$. The particle velocity at $\vec{r}_{m,q+1}$ is

$$\vec{v}_{m,q+1} = \vec{v}_{m,q} + \vec{g}\,\delta t. \tag{5}$$

We chose the time-step size such that the particle can only advance a maximum distance of $R_o/256$, within δt. Upon collision with the obstacle, the incident velocity $\vec{v}_k$ is decomposed into its tangential and normal components:

$$\vec{v}_k = \vec{v}_k^{(T)} + \vec{v}_k^{(N)}. \tag{6}$$

At the collision point with the obstacle or wall, the unit normal vector is defined as

$$\hat{n} = \vec{\nabla}Q(\rho,z)/|\vec{\nabla}Q(\rho,z)|, \tag{7}$$

such that $\vec{v}^{(N)} = (\vec{v}\cdot\hat{n})\hat{n}$ and $\vec{v}^{(T)} = \vec{v} - \vec{v}^{(N)}$, where "$\cdot$" represents a vector dot product. Immediately after collision, the normal velocity component changes as $\vec{v}^{(N)} \to -\mu_N \vec{v}^{(N)}$. The tangential component of the rebound velocity $\vec{v}^{(T)}$ remains unchanged in the absence of frictional effects, i.e., $\vec{v}^{(T)}$

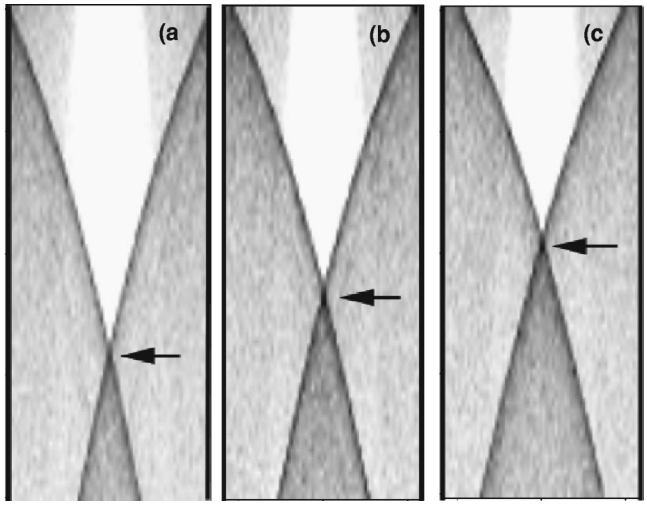

FIG. 2. Trajectories (flight path) of $M=10^4$ falling grains in the x-z plane ($R_c=3.5R_o$) for $\mu_N=0.8$ (a), 0.9 (b), and 1.0 (c). Arrows indicate the peak in the probability of passage through the transverse plane. The topmost part of the image is at $z=H+R_o$, which is directly below the obstacle whose center is at $z=H=2.0R_o$ below the entrance facet ($z=0$). The height of the cylindrical pipe is $15R_o$. A ''shadow'' region is seen immediately below the obstacle where trajectories are not found.

$\rightarrow\vec{v}^{(T)}$ [17,18]. All collisions of the mth particle with the wall are assumed to be elastic.

III. EXPERIMENTS

We consider the simpler case when the falling grains are infinitely small ($R_g=0$, $\mu_T=0$) and the collision cross section of the spheroid is equal to the entrance facet area ($R_e=R_o$). Viewed from the top, scattering cross section of the spheroid is πR_o^2. A total of M identical grains are released from rest at random initial positions (uniformly random distribution) in the entrance facet. In the absence of collisions with other grains, a falling grain remains in one and the same plane of incidence regardless of the number of collisions that it experiences with the obstacle or wall. The problem therefore, is two dimensional in character. All numerical calculations are done in double precision [$g++-$GNU project C and $C++$ Compiler (egcs-1.1.2)].

Focusing behavior of falling grains. We found that the trajectories of the falling grains are focused towards a point in the cylinder axis after colliding with the obstacle and the cylinder walls. A transverse plane $z=z_F$, can be found that shows a significant peaking in the arrival distribution at the axial region (see, Fig. 2). The focus locations ($x=0,z_F$) depends on the $\mu=\mu_N$ value.

Figure 3 presents profiles of the grain distribution at several transverse planes near the focal plane. Focusing reduces the uncertainty of the grain location from one part in $2R_o/\Delta x$ to one part in $2R_F/\Delta x$, where R_F ($\ll R_o$) is the radius of the central spot of the probability density distribution and Δx is the sampling interval (bin) in the x axis. We found that $2R_F\approx 4\Delta x$, regardless of the numerical value of Δx.

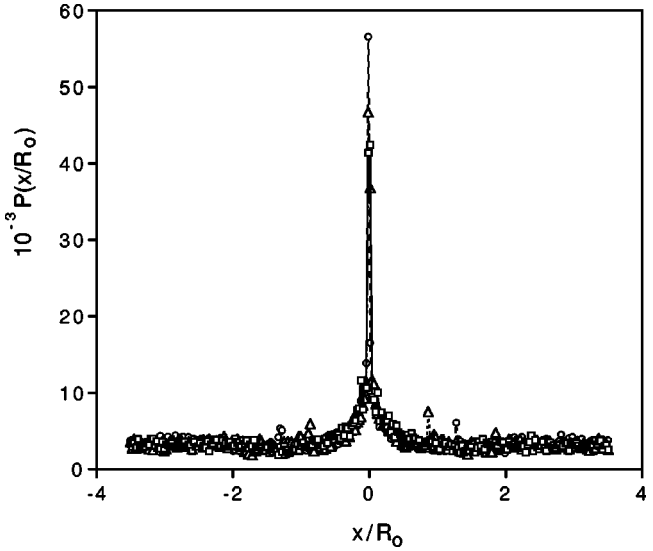

FIG. 3. Distribution $P(x/R_o)$ of landing positions ($\Delta x=2R_e/128\approx 0.055R_o$, $R_e=3.5R_o$, $H=2.0R_o$) near the focus plane $z=z_F=11.5R_o$. $P(x/R_o)$ represents the ratio between the number of grains incident at position x of the z plane and the total number of grains released at $z=0$. Three μ_N values are considered: 0.75 (circles), 0.85 (triangles), and 1.0 (squares).

Figure 4 plots the z_F value (circles) as a function of μ_N for $R_e=3.5R_o$, and in the range $0.7\leqslant\mu_N\leqslant 1.0$. The solid curve is described by $z_F=30(1-\mu_N)+9.6\mu_N^2$, which indicates that z_F increases nonlinearly with μ_N. A small change $\Delta\mu_N$ results in a translation of the focus position by $\Delta z_F\approx(19.2\mu_N-30)\Delta\mu_N$. Also plotted in Fig. 4 is the dependence of z_F (filled circles) with R_c. The solid curve is de-

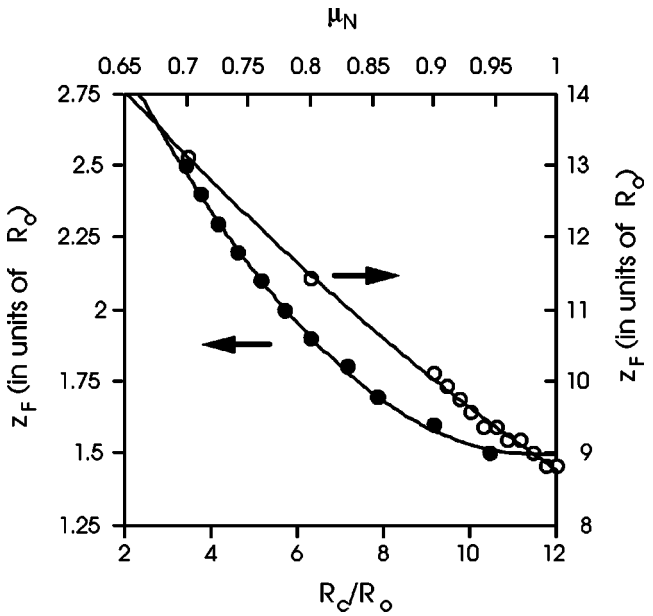

FIG. 4. Location of the focal plane $z=z_F$. Dependence of z_F (unfilled circles) with μ_N where $\Delta x=2R_e/128$, $R_e=3.5R_o$, $H=2.0R_o$. The solid curve is described by $z_F=30(1-\mu_N)+9.6\mu_N^2$. Also shown is the dependence of z_F (filled circles) with pipe radius $R_e(\mu_N=1,\ \Delta x=2R_e/128,\ H=2.0R_o)$.

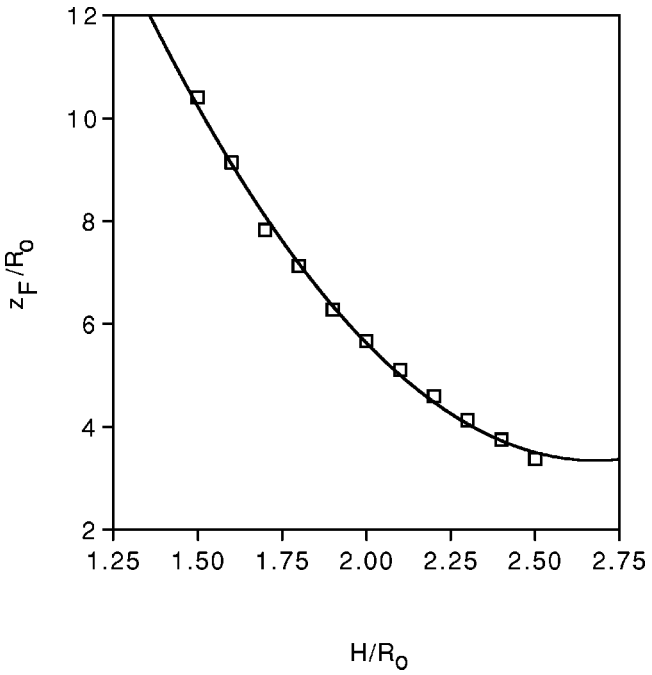

FIG. 5. Dependence of z_F (filled circles) with distance H of the obstacle from $z=0$ ($\mu_N=1$, $\Delta x=2R_e/128$, $R_e=3.5R_o$). The solid curve is described by $z_F=4.96H^2-26.58H+38.94$.

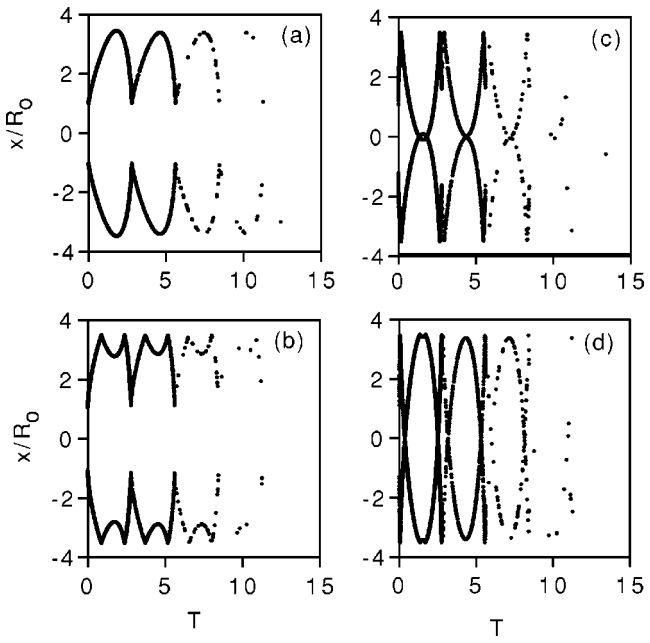

FIG. 6. Spheroid obstacle. Arrival positions x of falling grains as a function of T for $z=H$ (a), $H+R_o$ (b), $H+7R_o$ (c), $H+18R_o$ (d), where $-R_c\leqslant x\leqslant R_c$. Each plot contains the landing records of 10^3 grains that are released at random positions in the entrance facet ($R_e=3.5R_o$).

scribed by: $z_F=0.65R_c^2+1.1R_c-3.1$. A small change ΔR_c also causes the focus position to translate by $\Delta z_F\approx(1.3R_c+1.1)\Delta R_c$.

Figure 5 plots the dependence of z_F with axial position H of spheroid center from $z=0$. The solid curve is described by $z_F=4.96H^2-26.58H+38.94$. A small change ΔH results into a translation of the focus position by $\Delta z_F\approx(9.92H-26.58)\Delta H$. The results in Figs. 4 and 5 illustrate that the location of the focal plane is sensitive to variations in the values of μ_N, R_c, and H.

Time of flight. We also plot the values of the relative time of flight $T=t(z)-t_o$, where $t(z)$ is the time duration that it takes for a falling grain from the entrance facet ($z=0$), to reach a chosen z plane which is located below the obstacle, and t_o is the duration for the grain to reach the same z plane without the obstacle (collision-free free fall).

Figure 6 plots the landing locations x of the falling grains as a function of T for $z=H$ (a), $H+R_o$ (b), $H+7R_o$ (c), $H+18R_o$ (d), where $-R_c\leqslant x\leqslant R_c$. Each plot contains the arrival positions of 10^3 grains that are released at random positions in the entrance facet ($R_e=3.5R_o$). The $x(T)$ plots are degenerate and exhibits a periodic pattern with T. Their characteristics imply that in the absence of intergrain collisions, grains which are released simultaneously at randomly-selected locations in the entrance facet arrive at a chosen z plane at different times due to collisions with the obstacle and walls, which increase their flight times.

No grains are incident at regions near $x=0$ in Figs. 6(a) and 6(b). However, with increasing z from $z=H$ [Fig. 6(a)], $x(T)$ curves "expand" towards the cylinder walls ($x=\pm R_c$) and get "reflected" towards the opposite direction [Fig. 6(b)]. The tips of the two curves from the opposite sides eventually meet with each other at $x=0$, to form the focal plane at $z=z_F\approx H+7R_o$ [Fig. 6(c)]. Hence, the grain arrivals at the focal plane, are nonuniform in time and occurs in a series of bursts.

The presence of the massive obstacle introduces degeneracy into the allowed arrival positions at a chosen z plane for grains which are released randomly at the entrance facet. Figure 7 plots the arrival position x at $z=H+13R_o$, as a function of the release position x_o at $z=0$ with the cylindrical wall removed ($R_c\rightarrow\infty$). The $x(x_o)$ plot is highly periodic in the log scale of the x_o axis which implies that grains released at x_o and $x_o/10^s<1$, arrive at the same x-location in the plane: $z=H+13R_o$, where s is an integer.

Annular entrance facet. When the initial positions of the falling grains are restricted to within an annular region, $R_1<x_o<R_2$, the resulting transverse grain distribution at a transverse plane $z\neq z_F$, is also annular. At the focal plane, the grain distribution is more confined than that produced with a circular entrance facet. This is a direct consequence of the degeneracy of x with x_o as illustrated in Fig. 7.

Conic obstacle. We also investigated the effect of obstacle shape on the focusing behavior by considering a (massive) conic obstacle instead of the spheroid. The apex (part of obstacle nearest to the entrance facet) of the cone is located at $H=7R_o$, and the base radius is R_o. Viewed from the top, the scattering cross section of the conic is πR_o^2 which is equal to that of the spheroid that was considered earlier. Figures 8(a) and 8(b) present the grain trajectories for the following set of parameter values: ($H=9R_o$, $R_c=6R_o$, $\mu_N=1.0$) and ($H=10R_o$, $R_c=6R_o$, $\mu_N=1.0$), respectively. Unlike with the spheroid obstacle, focusing of the falling grains occurs only for a unique combination of values for H,

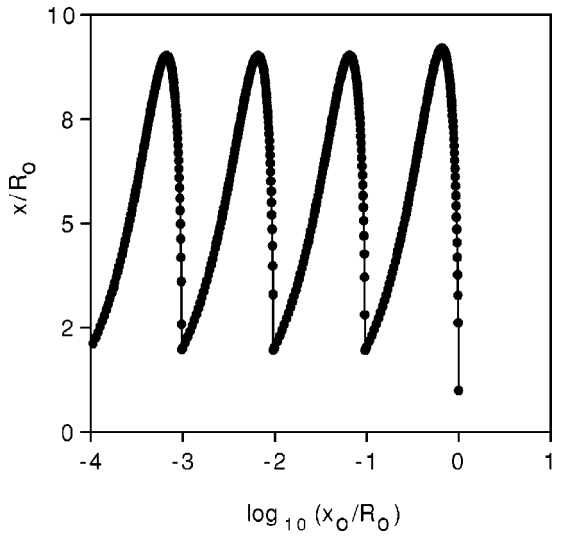

FIG. 7. Arrival positions x/R_o of falling grains at $z=H+15R_o$, as a function of release position x_o/R_o (in $\log_{10}$ scale) at the entrance facet $z=0$.

R_c, and μ_N. Deviations from the parameter combinations result in focusing failure. Table I lists the $H-R_c$ combinations ($\mu_N=1.0$) that yield a focused distribution at the plane $z=z_F$, for the conic obstacle of base radius R_o.

IV. DISCUSSION

A technique has been demonstrated that separates grains of the same mass and size but different coefficient of restitution μ. With a massive spheroid obstacle, the focusing of the falling grains is obtained. The separation process is efficient because at the focal plane, the grains are gathered over a very small area around the z axis even if they are released at random positions in the entrance facet. The process is also economical because it relies only on the force of gravity. For given R_o, R_c, R_e, and H values, focal plane location z_F exhibits a quadratic dependence with μ_N. The ability to resolve two closely-separated values μ_{N1} and μ_{N2}, is easier for grains with large μ_N's since $\Delta z_F \approx (19.2\langle\mu_N\rangle - 30)\Delta\mu_N$, where $\langle\mu_N\rangle = 0.5(\mu_{N1}+\mu_{N2})$, and $\Delta\mu_N = |\mu_{N1}-\mu_{N2}|$. The $z_F(R_c)$ plot in Fig. 4, reveals that the spheroid obstacle and the cylinder walls are necessary for focusing to happen for the spherical grains.

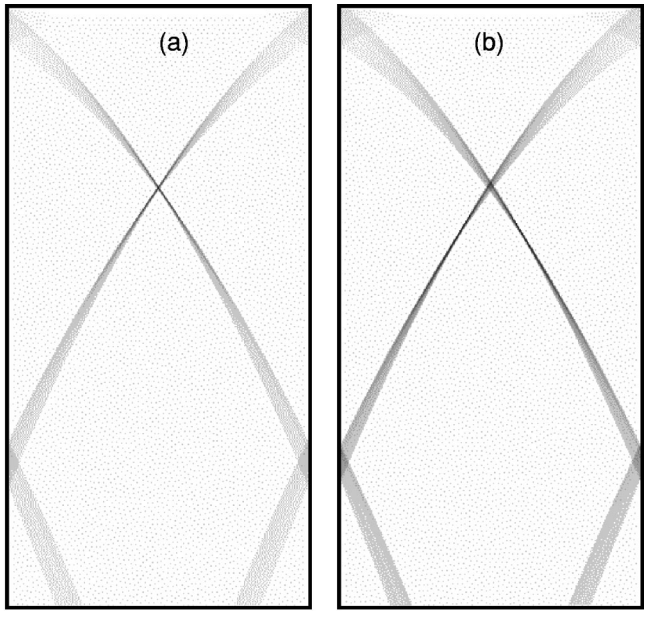

FIG. 8. Massive conic obstacle. Grain trajectories for $M=2\times10^3$ (a) $H=9R_o$, $R_c=6R_o$, $\mu_N=1.0$ and (b) $H=10R_o$, $R_c=6R_o$, $\mu_N=1.0$. The topmost and bottom parts of each image are $z=H+R_o$ and $z=20R_o$, respectively.

TABLE I. Conic obstacle. Combination of parameter values that leads to focusing of falling grains.

R_c/R_o	H/R_o	z_F/R_o
5	7.25	10.68
6	9.00	12.99
7	10.0	14.85
8	12.0	17.31
9	13.0	19.17

Grains arrive at the focal plane in ''bursts'' even if they are released simultaneously at the entrance facet provided that intergrain collisions are absent. Grains that leave the entrance facet from initial positions that are near to the cylinder axis are likely to undergo multiple bounces and their time of flights to the focus plane are longer than those released at positions which are far from the axis.

So far we have only considered dimensionless grains ($R_g=0$). The corresponding case of a finite-sized grain of radius $R_g>0$, may be understood by noting that in the absence of rotation (spin), its bounce behavior is equivalent to that of a dimensionless grain colliding with an obstacle of ''effective'' radius (R_o+R_g), and effective pipe radius of (R_c-R_o). Focusing may not occur in the presence of rotational motion for the falling grains when the kinetic energy is not totally utilized for the translational displacement of the center of mass of the grain.

The focusing behavior of the falling grains is dependent on the surface profile of the massive obstacle. With a spheroid, focusing is ensured for a large number of combinations for R_c and H values (see, Figs. 4 and 5). With a cone, focusing is only possible for specific values of R_c and H (see, Table I).

V. CONCLUSIONS

We have presented a simple configuration that leads to the high-resolution separation of grains of similar mass and size but different elastic properties. Falling grains are focused at points on the cylinder axis according to the relative values of their coefficient of friction.

ACKNOWLEDGMENT

The project is partially supported by the Commission on Higher Education of the Philippines.

[1] P. de Gennes, Rev. Mod. Phys. **71**, s374 (1999).
[2] T. Shinbrot and F. Muzzio, Phys. Today **53**(3), 25 (2000).
[3] N. Burtally, P. King, and M. Swift, Science **295**, 1877 (2002).
[4] A. Rosato, D. Blackmore, N. Zhang, and Y. Lan, Chem. Eng. Sci. **57**, 265 (2002).
[5] D. Rapaport, Phys. Rev. E **64**, 061304 (2001).
[6] S. Aumaitre, C. Kruelle, and I. Rehberg, Phys. Rev. E **64**, 041305 (2001).
[7] K. Choo, T. Molteno, and S. Morris, Phys. Rev. Lett. **79**, 2975 (1997).
[8] M. Möbius, B. Lauderdale, S. Nagel, and H. Jaeger, Nature (London) **414**, 270 (2001).
[9] D. Brone and F. Muzzio, Phys. Rev. E **56**, 1059 (1997).
[10] T. Shinbrot, A. Alexander, and F. Muzzio, Nature (London) **397**, 675 (1999).
[11] E. Falcon, R. Wunenburger, P. Evesque, S. Fauve, C. Chabot, Y. Garrabos, and D. Beysens, Phys. Rev. Lett. **83**, 440 (1999).
[12] T. Shinbrot, Nature (London) **389**, 574 (1997).
[13] S. Dippel, G. Batrouni, and D. Wolf, Phys. Rev. E **54**, 6845 (1996).
[14] M. Scherer, T. Mahr, A. Engel, and I. Rehberg, Phys. Rev. E **58**, 6061 (1998).
[15] L. Vanel, A. Rosato, and R. Dave, Phys. Rev. Lett. **78**, 3640 (1997).
[16] A. Lue and H. Brenner, Phys. Rev. E **47**, 3128 (1993).
[17] B. Painter and R. Behringer, Phys. Rev. E **62**, 2380 (2000).
[18] N. Brilliantov, F. Spahn, J. Hertzsch, and T. Pöschel, Phys. Rev. E **53**, 5382 (1996).